# **CONFERENCE PRE-PRINT**

# HIGH PERFORMANCE ELM-FREE SEMI-DETACHED SCENARIO SUSTAINED AT HIGH-CURRENT IN JET DTE3

C. Giroud<sup>1</sup>, D.B. King<sup>1</sup>, I.S. Carvalho<sup>2</sup>, D. L. Keeling<sup>1</sup>, L. Frassinetti<sup>3</sup>, R. A. Pitts<sup>2</sup>, G. Pucella<sup>4</sup>, S. Wiesen<sup>5</sup>, A. Kappatou<sup>6</sup>, N. Vianello<sup>7,16</sup>, M. Wischmeier<sup>6</sup>, F. Rimini<sup>1</sup>, M. Baruzzo<sup>4,7</sup>, M. Maslov<sup>1</sup>, M. Sos<sup>8</sup>, X. Litaudon<sup>9</sup>, R. B. Henriques<sup>1</sup>, K. Kirov<sup>1</sup>, C. Perez von Thun<sup>10</sup>, H. J. Sun<sup>1</sup>, P. Dumortier<sup>11</sup>, E. Lerche<sup>11</sup>, P. Jacquet<sup>1</sup>, M. Lennholm<sup>1</sup>, J. Mitchell<sup>1</sup>, A. Parrott<sup>1</sup>, J. Bernardo<sup>1</sup>, M. Zerbini<sup>4</sup>, I. Coffey<sup>1,12</sup>, K. Collie<sup>1</sup>, J. M.Fontdecaba<sup>13</sup>, N. Hawkes<sup>1</sup>, Z. Huang<sup>1</sup>, I. Jepu<sup>1</sup>, D. Kos<sup>1</sup>, K. Lawson<sup>1</sup>, E. Litherland-Smith<sup>1</sup>, A. Meigs<sup>1</sup>, C. Olde<sup>1</sup>, A. Patel<sup>1</sup>, L. Piron<sup>7,14</sup>, M. P. Poradzinski<sup>1,10</sup>, F. Eriksson<sup>1</sup>, Z. Stancar<sup>1</sup>, D. Taylor<sup>1</sup>, E. Alessi<sup>16</sup>, I. Balboa<sup>1</sup>, A. Boboa<sup>1</sup>, S. Bakes<sup>1</sup>, M. Brix<sup>1</sup>, E. De la Cal<sup>13</sup>, P. Carvalho<sup>1</sup>, A. Chomiczewska<sup>10</sup>, J. Eriksson<sup>15</sup>, Z. Ghani<sup>1</sup>, E. Giovannozzi<sup>4</sup>, J. Foster<sup>1</sup>, A. Huber<sup>17</sup>, J. Karhunen<sup>18</sup>, E. Kowalska-Strzeciwilk<sup>10</sup>, K. Lawson<sup>1</sup>, J. Maddock<sup>1</sup>, J. Matthews<sup>1</sup>, S. Menmuir<sup>1</sup>, K. Mikszuta-Michalik<sup>10</sup>, R. B. Morales-Bianchetti<sup>1</sup>, D. Moulton<sup>1</sup>, M. Nocente<sup>19</sup>, E. Pawelec<sup>20</sup>, E. Pinto<sup>13</sup>, D. Refy<sup>21</sup>, P. Ryan<sup>1</sup>, I. Voldiner<sup>13</sup>, G. Sergienko<sup>17</sup>, S. Silburn<sup>1</sup>, G. Stankunas<sup>22</sup>, C. Silva<sup>23</sup>, J. Svodoba<sup>8</sup>, G. Szepesi<sup>1</sup>, M.Tomes<sup>8</sup>, B. Thomas<sup>1</sup>, A. Tookey<sup>1</sup>, Y. Zayachuk<sup>1</sup>, N. Wendler<sup>10</sup>, L. Xiang<sup>1</sup>, F. Aurienma<sup>7,28</sup>, I. Borodkina<sup>8</sup>, D. Fajardo<sup>6</sup>, A. Fil<sup>9</sup>, S. Gabriellini<sup>1</sup>, L. Garzotti<sup>1</sup>, S. Henderson<sup>1</sup>, Q. Hu<sup>16,19</sup>, P. Innocente<sup>7</sup>, I. Ivanova-Stanik<sup>10</sup>, A. Jarvinen<sup>18</sup>, H. Kumpulainen<sup>17</sup>, C. Leoni<sup>24</sup>, J. Lombardo<sup>7</sup>, P. Mantica<sup>16</sup>, A. Mariani<sup>16</sup>, M. Marina<sup>26</sup>, A.H. Neilsen<sup>27</sup>, H. Nystrom<sup>3</sup>, M. O.Mullane<sup>1</sup>, O. Pan<sup>6</sup>, V. Parail<sup>1</sup>, I. Predebon<sup>7,16</sup>, S. Saarelma<sup>1</sup>, J. Seidl<sup>8</sup>, E.R. Solano<sup>13</sup>, A. Stagni<sup>7</sup>, A. Thrysoe<sup>27</sup>, M. Valovic<sup>1</sup>, A. Widdowson<sup>1</sup>, V.K. Zotta<sup>24</sup>, JET Contributors\* and the EUROfusion Tokamak Exploitation Team\*\*.

<sup>1</sup>UKAEA, Culham Campus, Abingdon OX14 3DB, UK; <sup>2</sup>ITER Organization, Route de Vinon-sur-Verdon, CS 90 046, 13067 St Paul Lez Durance Cedex, France; <sup>3</sup>Division of Electromagnetic Engineering and Fusion Science, KTH Royal Institute of Technology, SE-10044 Stockholm, Sweden; <sup>4</sup> Nuclear Department - ENEA C. R. Frascati - via E. Fermi 45, 00044 Frascati (Roma), Italy; 5DIFFER - Dutch Institute for Fundamental Energy Research, De Zaale 20, 5612 AJ Eindhoven, Netherlands; Max-Planck-Institut für Plasmaphysik, Garching, Germany; Consorzio RFX, Corso Stati Uniti 4, Padova, 35127 Italy; Sinstitute of Plasma Physics of the Czech Academy of Sciences, U Slovanky 2525/1a, 182 00 Prague 8, Czechia; <sup>9</sup>CEA, IRFM, F-13108 Saint Paul Lez Durance, France; <sup>10</sup>Institute of Plasma Physics and Laser Microfusion, Hery 23 Street, 01-497 Warsaw, Poland; <sup>11</sup>Laboratory for Plasma Physics LPP-ERM/KMS, B-1000 Brussels, Belgium; 12 Astrophysics Research Centre, School of Mathematics and Physics, Queen's University, Belfast, BT7 1NN; <sup>13</sup>Laboratorio Nacional Fusión. CIEMAT. Av Complutense 40. 28040 Madrid. Spain; <sup>14</sup>Dipartimento di Fisica "G. Galilei", Università degli Studi di Padova, Padova, Italy; 15 Department of Physics and Astronomy, Uppsala University, Regementsvägen 10, 75137 Uppsala; 16 Institute for Plasma Science and Technology, CNR, 20125 Milano, Italy; <sup>17</sup> Institute of Fusion Energy and Nuclear Waste Management–Plasma Physics, Forschungszentrum Jülich GmbH, Germany; <sup>18</sup>VTT Technical Research Centre of Finland, P.O. Box 1000, 02044 VTT, Finland; <sup>19</sup>Department of Physics, University of Milano-Bicocca, Milan, Italy; Institute of Physics, University of Opole, Oleska 48, 45-052 Opole, Poland; Center for Energy Research, 29-33 Konkoly Thege Miklós street 1121 Budapest, Hungary; <sup>22</sup>Lithuanian Energy Institute, Laboratory of Nuclear Installation Safety, Breslaujos Str. 3, LT-44403 Kaunas, Lithuania; <sup>23</sup>Instituto de Plasmas e Fusao Nuclear, Instituto Superior Técnico, Universidade de Lisboa, 1049-001 Lisboa, Portugal; <sup>24</sup>Sapienza University of Rome, Rome, Italy; <sup>26</sup>Ecole Polytechnique Federale de Lausanne (EPFL), Swiss Plasma Center (SPC), Lausanne, Switzerland; 27PFFE, DTU Physics, Technical University of Denmark, 2800 Kgs. Lyngby, Denmark; 28Institute for Plasma Science and Technology, CNR, 35127 Padova, Italy; \*See the author list of CF. Maggi et al., Nucl. Fusion 2024, 10.1088/1741-4326/ad3e16, \*\*see the author list of E. Joffrin Nuclear Fusion 2024 10.1088/1741-4326/ad2be4 e-mail: carine.giroud@ukaea.uk

#### **Abstract**

Recent experiments on JET with the ITER-like wall (JET-ILW) have advanced core—pedestal—exhaust integration at plasma currents of 2.5–3.2 MA, supporting the ITER Q = 10 baseline and future D–T devices. Using a high-triangularity baseline and closed divertor in vertical divertor configuration, the so-called JET-ITER baseline, neon seeding enabled radiative divertor operation with partial detachment whilst improving confinement. Sustained plasmas with high neon content were maintained over several confinement times without active detachment control, aided by low tungsten levels and stationary conditions in both D–D and D–T regimes. These results provide key data for physics-based extrapolation to ITER, clarifying access, sustainment, and the coupled behaviour of core, pedestal, and exhaust under optimized impurity seeding.

## A. INTRODUCTION

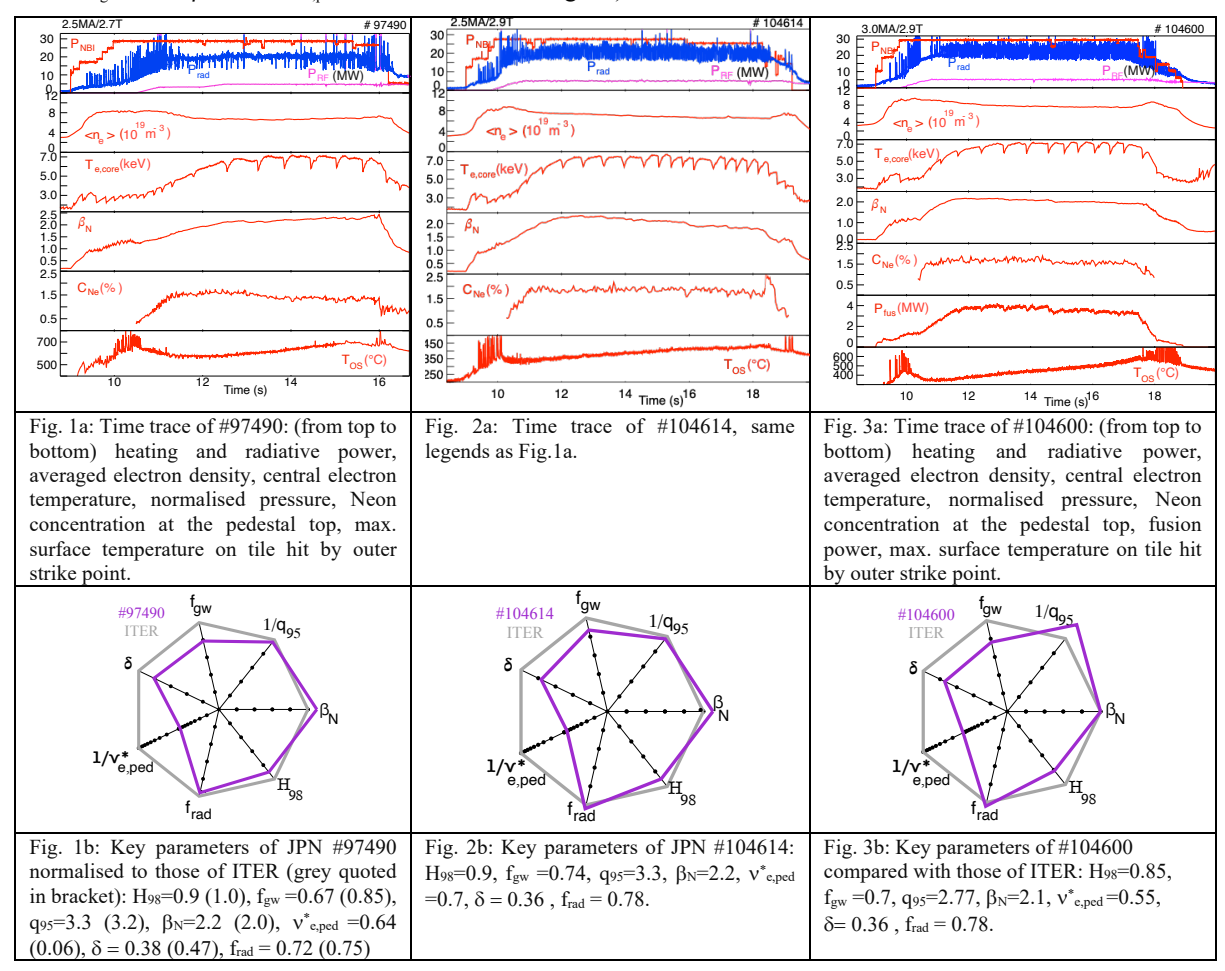
Recent advances in core-pedestal-exhaust integration at high plasma current in JET with tungsten (W) divertor and a beryllium (Be) first wall are vital in support of robust achievement of the ITER Q =10 baseline scenario and provide unique insights for the design of the next step D-T devices, including DEMO and STEP. A viable exhaust solution for a reactor-grade plasma must sustain a high radiative fraction (f<sub>rad</sub>) - achieved through injection of extrinsic impurities - to dissipate the power flux in the scrape-off layer (SOL) and divertor regions which would otherwise lead to intolerable divertor target heat fluxes [1]. Simultaneously, a sufficiently hot pedestal must be maintained to ensure good energy confinement, above the H-mode power threshold, ideally without Edge Localised Modes (ELMs), but with particle control and minimising main chamber erosion from fast ion and chatge-exchange (CX) neutral sputtering.

Over the 2022-2023, dedicated "JET-ITER baseline" experiments have been performed in D and in D-T while approaching the core-edge-exhaust integration conditions required for ITER baseline plasmas [2,3]. These plasmas are developed at high input power ( $P_{in}$  =30-35MW), with high plasma current ( $I_p$ =2.5-3.2MA) and with a magnetic configuration close to that of ITER: high triangularity ( $\delta_u$ =0.36-0.4,  $\delta_l$ =0.35),  $q_{95}$  =2.7-3.3, with a closed divertor with both strike points positioned on the vertical W divertor tiles (VV configuration, inertially cooled). Partial divertor detachment - an essential requirement for protecting the ITER divertor against high-heat flux under burning plasma conditions - is reached and sustained by injecting neon (Ne) (as foreseen on ITER) under feedforward conditions. Simultaneously, low pedestal collisionality is reached ( $v^*_{e,ped}$ ~0.3-0.4), at ITER baseline normalised pressure values ( $\beta_N$  ~2.1), and with small/no ELMs ( $\Delta T_{OuterTarget.max}$ <20°C,  $W_{ELM}/W$ <0.3%). These experiments provide crucial data for physics-based extrapolation of JET results to ITER and beyond, helping to understand the access and sustainment conditions, operational domain and the complex interplay of the underlying physics governing core, pedestal and exhaust integration.

#### 2. HIGH-PERFORMANCE CORE-EDGE INTEGRATED SCENARIO AT HIGH PLASMA CURRENT

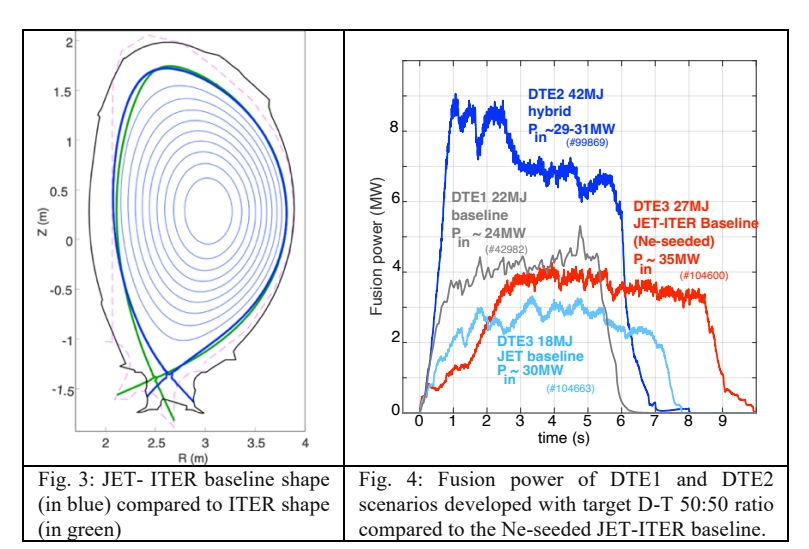
Efforts to develop a core-edge integrated scenario at JET with high confinement and neon seeding started a few year after the installation of the JET-ILW. The performance of these discharges remained low with a partially detached divertor [4] until additional power was available just before DTE2. Encouraging results showed the glimpse of a tantalising no-ELM high-performance with low target  $T_e$  at 2.5MA/2.7T ( $\beta_N$ =2.2;  $H_{98(y,2)}$ =0.9 with fast ion contribution removed [5],  $T_{e,OS}$  <5eV). These conditions were sustained for 4s without tungsten (W) accumulation and without ELMs, see Fig. 1a, and with an overall performance close to the ITER 15MA target at a power with 2xP<sub>LH</sub> (the power threshold for the L-H transition from [6]), see Fig 1b. The details of the magnetic configuration used is seen in Fig 3. Since last IAEA-FEC, it was confirmed that not only this is a robust scenario in D-D, but it can also be obtained in D-T [5,7]. Minimal adaptation of the D-D JET-ITER baseline scenario was required to reproduce the main results in D-T. High-performance plasmas were achieved in D-T at 2.5MA, with  $\beta_N$  reaching up to 2.5, with similarly high fr<sub>rad</sub> and high performance achieved with and without ELMs (JPN JPN (JET pulse number) #104614, 2.5MA, q<sub>95</sub>=3.3, P<sub>in</sub>=32.5MW, H<sub>98(y,2)</sub>=0.9, f<sub>gw</sub>=0.74, β<sub>N</sub> ~2.1, ν\*<sub>e,ped</sub>~0.6, no ELMs, see Fig. 2a,b), approaching the pedestal collisional domain expected in ITER.

Prior to DTE3, significant efforts were placed to expand the operation domain of the JET-ITER baseline towards lower collisionality and higher current (3.0-3.2MA,  $q_{95}$ =2.7-3.3). Operation at high current with a high-triangularity shape is technically very challenging, due to the high disruption forces (~4 MN even with mitigation) [3], even with mitigation, and was not attempted before in JET. It was established that the operational space at 3MA ( $q_{95}$ =2.7) and 3.2MA ( $q_{95}$ =3.2) [8] for high confinement and partially detached divertor was not accessible in D-D operation, but it could be reached with D-T operation at 3MA ( $q_{95}$ =2.7). For the first time, a Ne-seeded integrated scenario at 3MA in D-T with partially detached divertor has been achieved in stationary conditions for up to 6.5s (29 x  $\tau_E$ ), with fusion power of 4MW and without ELMs (JPN #104600, 3MA,  $q_{95}$ =2.7,  $P_{in}$ =34MW,  $H_{98(y,2)}$  = 0.85,  $f_{gw}$ =0.75,  $\beta_N$  ~2.1,  $v_{e,ped}^*$ ~0.5, no ELMs, see Fig. 3b).

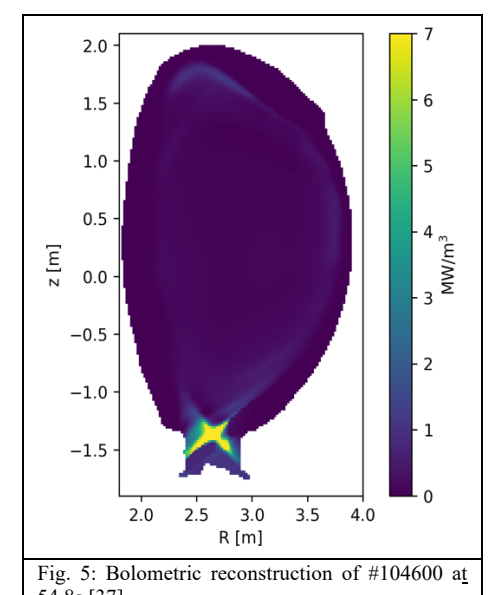


As shown in Figs. 1–3a, neon seeding in highly fuelled JET-ITER baseline plasmas produces similar effects in D–D and D–T. It reduces plasma density and gradually decreases ELM size (discussed later). Stationary conditions can be sustained for several confinement times even in ELM-free regimes s. 1a, 2a, 3a). At 3.2 MA with  $q_{95} = 3.2$ , plasmas remain in L-mode under neon seeding yet still exhibit density reduction [8].

**Fusion power:** Scenarios developed for high fusion power in DTE2 (all unseeded), with a 50:50 D-T ratio, are shown in Fig. 4, together with the



highest fusion energy achieved with ELMy H-modes in DTE1. The Ne-seeded 3MA D-T JET-ITER baseline plasma (#104600) produced 27 MJ, exceeding the DTE1 record (22 MJ), reaching within a factor of two of the 50:50 hybrid scenario fusion power, and exhibiting stationary conditions [34]. No attempt was made to increase the fusion power, as the focus of the study was core-edge-exhaust integration. The fusion power and energy of the seeded ITER baseline D-T pulses represent a notable achievement given the low-pumping divertor configuration (VV) and the high rates of fuelling and impurity seeding. All D-T JET-ITER baseline pulses were developed with a target 50:50 core fuel ratio, guided by edge D:T measurements [9-11]. In DTE3, however, the use of deuterium beams resulted in a core mix of  $n_T/(n_T+n_D) < 0.5$ , as also observed in the JET baseline scenario in DTE3 [12] (scenario with low triangularity and a plasma configuration optimising pumping which was extensively developed for high fusion power production in DTE2). JETTO-QuaLiKiZ core integrated modelling solved the particle balance with the effect of core fuelling with D-beams and estimated a ratio  $n_T/(n_T+n_D)$  could be between 0.3 and 0.45 [13]. Using the measured kinetic profiles, estimated impurity mix, and the predicted core isotopic ratio, TRANSP calculations reproduce the neutron rate within a factor of 1.3 of the measured value, whereas assuming a 50:50 D–T ratio would overestimate it by a factor of two or more. For  $0.3 < n_T/(n_T+n_D) < 0.00$ 0.45, the ratio of thermal to beam-target neutron emission predicted by TRANSP is consistent with values inferred from neutron spectroscopy using the diamond detector [34,35] and thin-foil magnetic proton recoil spectrometer [14,15]. The 4 MW fusion power measured in the record 3 MA Ne-seeded JET-ITER baseline plasma (#104600) was approximately one-third thermal (TH) and two-thirds beam-target (BT) neutron contributions, consistent with the TH/BT ratio observed in the JET baseline DTE2 assessment [16]. These results are in contrast with the expected fast isotope mixing [17], and further investigation is required to understand the apparent discrepancy.



W content: The W content remains low in the Neon-seeded JET-ITER baseline plasmas which allows, together with mild MHD [22], stationary plasma conditions. The tomographic reconstruction of #104600 (typical of the Ne-seeded JET-ITER baseline plasmas) does not show high radiation region on the low-field side (Fig. 5), unlike the hybrid or JET-baseline plasmas [17]; the radiation is localised at the divertor both below and above the X-point. The W content remains below  $C_W < 1x10^{-4}$  within the confined plasma. When ELMs are present, W is mostly eroded in the inter-ELM phases by Ne impurity ions with a gross W erosion higher than for unseeded plasmas [18]. Some improved W screening is occurring either in the SOL - where a balance between the temperature gradient force, friction force, prompt W redeposition, and the divertor target sheath electric field determines W transport – or in the pedestal, where a large ion temperature gradient combined with low-density gradient reverses the neoclassical convection outward, reducing W content across the pedestal. With a high pedestal ion temperature gradient and low pedestal density (shown later) in the high Ne-seeded JET-ITER baseline, some degree of W screening in the pedestal, could be anticipated. In fact, detailed NEO

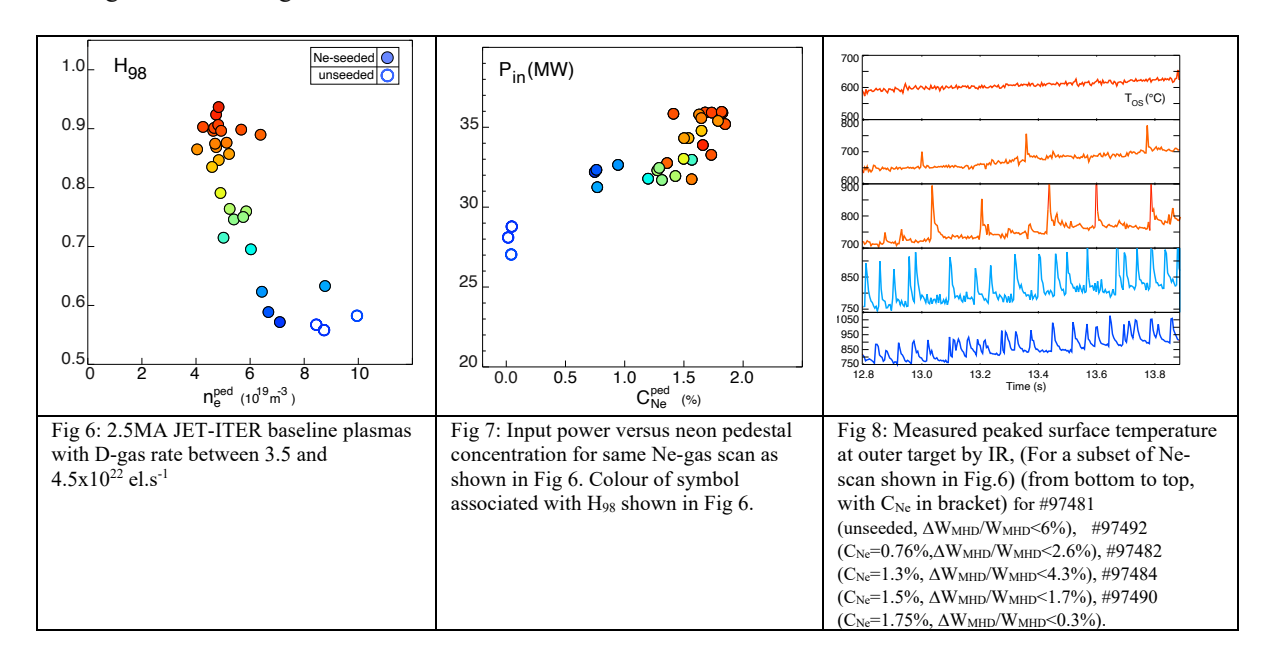
simulation [19], in #97490, show that the Ne-seeded pedestal is in the collisionality range where rotation decrease and even reverse the effect of the temperature screening [20]. In other words, the neoclassical W convection is inward. This means that only the W screening in the SOL can mitigate the core W content. Initial ERO2.0 W

erosion and edge transport with JINTRAC W core transport suggest that the JET-ITER baseline could achieve low W content due to low pedestal density gradient, effective W screening in the SOL owing to a wide, high-density ionising SOL and a low W source in the absence of ELMs [21].

Core MHD: Ne-seeding was observed to impact sawtooth (ST) behaviour. With increased central electron temperature, the ST period nearly doubled (0.3–0.6 s) and the inversion radius increased by ~10%. Inter-ST m/n = 1/1 MHD fluctuations also increased in amplitude and frequency [22]. Despite the long ST periods and high-performance operation, neoclassical tearing mode (NTM) activity remained mild, with only high-n NTMs (n=4,5,6) appearing in discharges with optimised access. The n=4 mode, present in most Ne-seeded JET-ITER baseline plasmas, reduced stored energy by less than 5% and was associated with decreased inter-ST 1/1 amplitude and shorter ST periods. An n=3 NTM appeared when neon injection and the associated  $\beta_N$  rise were too rapid, while the performance-limiting n=2 NTM occurred only in non-optimised H-mode access with long initial ST periods prior to Ne-seeding.

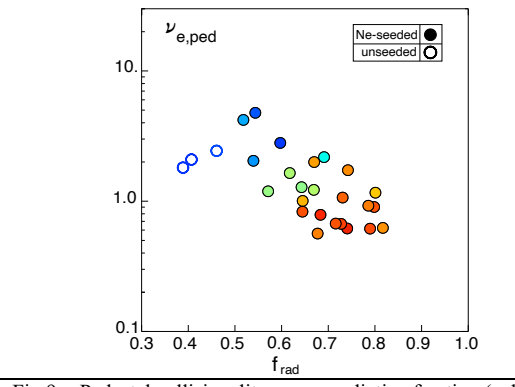
#### 3. OPERATIONAL DOMAIN OF JET-ITER BASELINE AND IDENTIFICATION OF KEY TRENDS

The focus of the high-performance integrated scenario is to provide an understanding of the core-edge-SOL integration in scenario close to the edge parameters of ITER, to offer a unique database to validate first principle and integrated modelling suite of code. For this reason, particular attention was given to obtain well-diagnosed plasmas in the divertor, SOL, pedestal and core, and to study the details of the core-edge integration at various fuelling and Ne-seeding level and divertor conditions with and without ELMs.



As already reported in [5], the increase in Ne-seeding in the JET-ITER baseline plasmas results in an increase in stored energy and confinement as shown in Fig. 6 (and neutron rate, not shown), in the 2.5MA D-D plasmas with a gas-rate between 3.5-4.5x10<sup>22</sup> el.s<sup>-1</sup>. The decrease in average electron density (n<sub>e</sub>) is due to a decrease of the pedestal  $n_e$  as shown in Fig. 6. A threshold in terms of Ne concentration ( $C_{Ne} \gtrsim 1.3$  %) at fixed input power ( $P_{in} \sim 31MW$ ) is also clearly seen in Fig 7. The high confinement is obtained at the highest input power (Pin=33-35MW). We will see later how these two thresholds can be re-interpreted in terms of ne.sep and Psep (electron separatrix density and power flowing through the separatrix in the pre-ELM phase, respectively). An additional characteristic is that the ELM size is reduced as the C<sub>Ne</sub> increases and even disappear at high input power and C<sub>Ne</sub>, see Fig.8. The reduction of the pedestal density would lead naturally to an increase of the pedestal temperature, with an assumed constant pedestal pressure. With a decreased pedestal collisionality, the ne core peaking is increased leading to a higher core contribution to the total stored energy. Fig. 9 illustrates that the pedestal collisionality can be decreased down to about 0.5, closer to the ITER domain of ve\*<0.1; however, this alone is insufficient to achieve high-performance at high radiative fraction. An increased pedestal pressure (ptot) is required for H<sub>98</sub>>0.8 (Fig. 10). The increased pedestal pressure is due to an increased ion and electron temperature, see Fig. 11. As the radiative fraction (calculated taking the energy balance in consideration [7]) is increased towards divertor detachment with neon seeding, the pedestal temperatures at about 0.8keV with a ratio T<sub>i,ped</sub>/T<sub>e,ped</sub>=1 in unseeded plasma, increase up to values of T<sub>i,ped</sub>=2.4keV And T<sub>e,ped</sub>=1.6keV (T<sub>i</sub>/T<sub>e</sub>=1.5) at max input power and C<sub>Ne</sub>. The increased value of T<sub>i</sub>/T<sub>e</sub> is likely to influence the pedestal transport as will be clarified

in section 4. The increase in pedestal height is not due to an increase in the gradient, which remains constant, but due to a widening of the pressure pedestal. This widening is mainly due to an inward shift of the electron temperature and a widening of the ion temperature (not shown) [23][24]



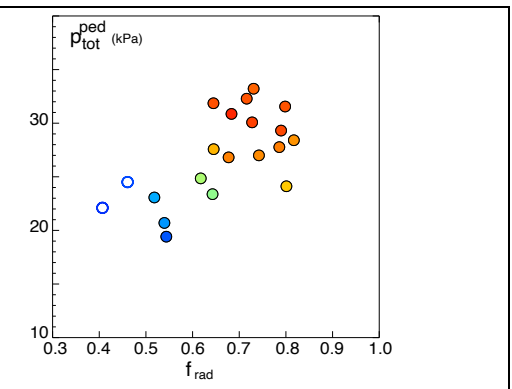


Fig 9: Pedestal collisionality versus radiative fraction (calculated taking the energy balance in consideration) for Ne-scan shown in Fig.1. The colour is related to the H<sub>98</sub> value for each discharge, see Fig 6

Fig 10: Total pedestal pressure versus radiative fraction, for scan shown in Fig 1. The colour is related to the H<sub>98</sub> value for each discharge, see Fig 6.

The improvement in confinement during the initial Ne scan at constant input power [5] was investigated using JINTRAC-QuaLiKiz [25] and attributed primarily to increased pedestal temperature, with ExB shear and dilution contributing to a lesser, but comparable, extent. A similar assessment has been done with an additional JINTRAC-QuaLiKiz study on the Ne-scan with increasing input power, shown in Fig. 7. Even if higher toroidal rotation and  $C_{Ne}$  have an impact in stabilizing turbulent diffusion inside the core ( $\psi_n$ <0.8), most of the increment in confinement properties originates from the increase in pedestal pressure and temperature [26]. In [27] with JINTRAC-TGLF, it was shown that the addition of neon in the core-transport only provide an increase of 10% in the confinement. In general, core integrated modelling can capture the key feature of the JET-ITER baseline. Details of the change of pedestal transport, stability and operation mode of the pedestal needs to be investigated further.

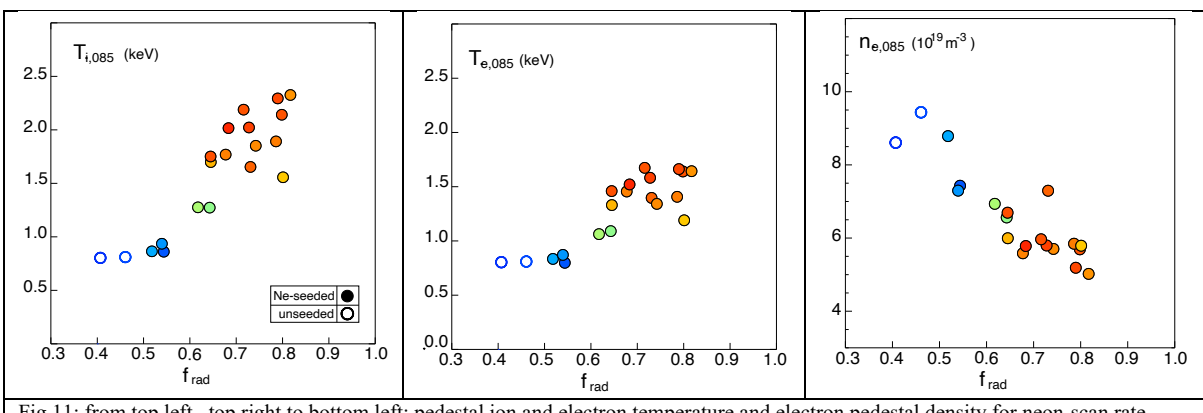
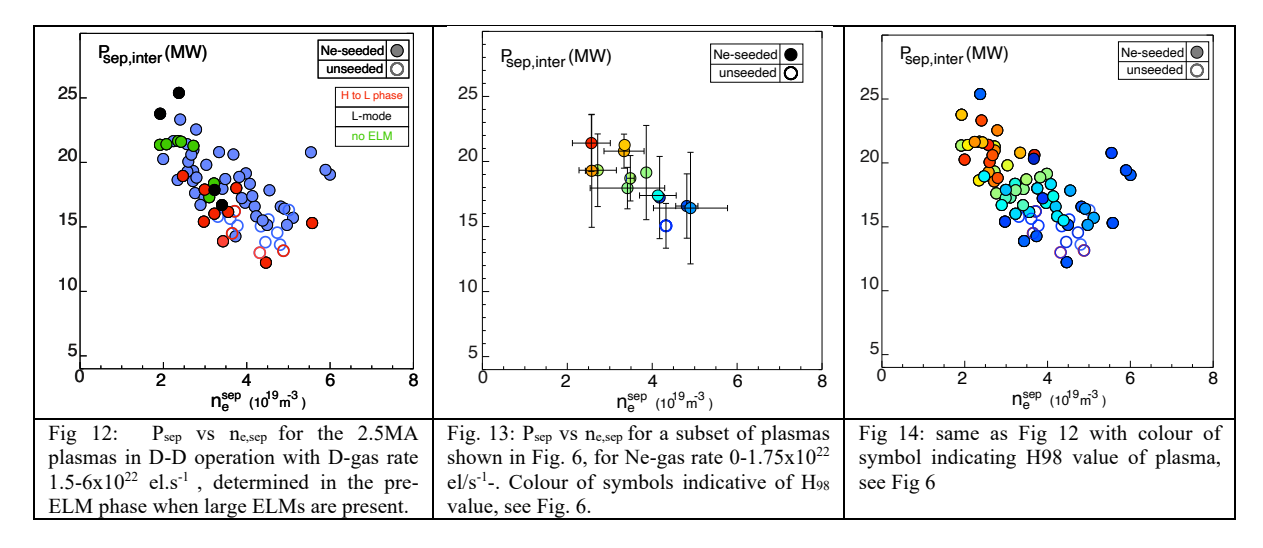


Fig 11: from top left, top right to bottom left: pedestal ion and electron temperature and electron pedestal density for neon-scan rate shown in Fig. 6. Colour related to the H<sub>98</sub> of each shot as shown in Fig 6.

Operational space with respect to the L-H power threshold: The operational domain of the JET-ITER plasma is explored in terms of the H-L transition, its variation between D-D and D-T operation, and its dependence on plasma current. The operational space was characterised in terms of P<sub>sep</sub> versus n<sub>e,sep</sub> (n<sub>e,sep</sub> calculated from power balance [28][29], inspired from description in [36]) for all JET-ITER plasmas obtained at 2.5MA with gas-rate from 1.5-6x10<sup>22</sup> el.s<sup>-1</sup>, with good and poor confinement plasmas, see Fig.12. As no dedicated P<sub>LH</sub> studies have been carried out for this configuration, the only way to identify the high and low density PLH branch ( even if less precise than a dedicated PLH study) is to mark out the discharges with clear back-transition from H-L (no hysteresis is expected, P<sub>LH</sub> expected equal to P<sub>HL</sub>) obtained in the JET-ITER baseline either seeded or unseeded, shown in red in Fig.12. It highlights that the unseeded plasmas naturally occur in the density region where PLH is minimum. An illustration of the trajectory followed by subset of the Ne-scan (shown in Fig. 6 and 7) done on the same day, is shown Fig. 13. As the neon-seeding rate is increased, ne,sep decreases and Psep increases. Psep (=Pin-dW/dt-Prad,core, W being the stored energy,  $P_{in}$  the input power) tends to increase even at constant  $P_{in}$  due to the reduction of the dW/dt term with Neon-seeding (decreased ELM size), even after accounting for the core radiation. From fig. 13, a picture emerges. As Ne-seeding rate is increased, the n<sub>e,sep</sub> is reduced [1,5], moving the plasma towards the low density P<sub>LH</sub> branch. If P<sub>sep</sub> is not sufficient, the plasma will enter a zone with a hard transition from H to L, and poor confinement, see Fig. 13. If P<sub>sep</sub> is sufficiently high as the neon-seeding rate is increased, the plasma can reach a zone, at proximity to the low-density branch (known for a smooth transition from H to L), in a domain of no-ELM and high confinement, i.e.  $P_{sep} / P_{LH} > 1.25$  and  $n_{e,sep} = 2-2.5 \times 10^{19}$  m<sup>-3</sup>. The operational domain for high-confinement, ELM-free D-T plasmas at 2.5MA is similar in terms of  $P_{sep}$  and  $n_{e,sep}$  (not shown). Due to a ~20% lower power threshold in D–T compared with D [31], the 2.5 MA D–T plasma did not fully test access to this state. Confirmation is provided by 3 MA D–T plasmas, which reach this operational domain—unattainable in 3 MA D–D— at  $P_{sep} / P_{LH} > 1.25$  and  $n_{e,sep} = 2-2.5 \times 10^{19}$  m<sup>-3</sup> (not shown). While not directly applicable to ITER, these results provide insight into processes that can occur with impurity seeding in ITER plasmas at higher current at proximity to the L-H power threshold.



#### 4. INTEGRATED SCENARIO: COMPLEX PICTURE OF INTERCONNECTED PHENOMENA

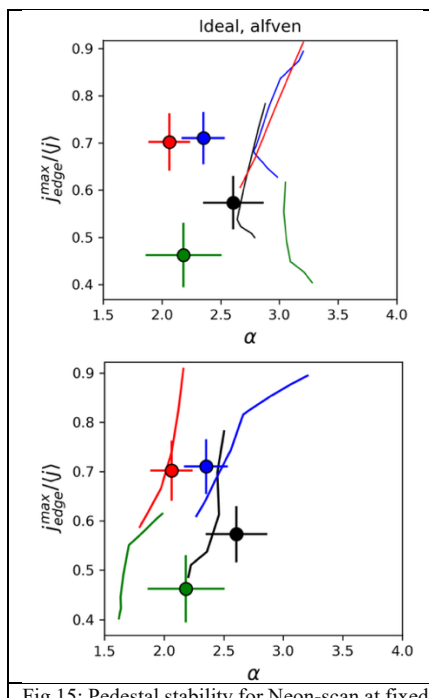


Fig 15: Pedestal stability for Neon-scan at fixed D-gas: top ideal MHD with Alfven criterion, bottom resistive MHD for unseeded (#97481, back), seeded (C<sub>Ne</sub>) #97492 (0.76%, green), #97482 (1.3%, blue), #97490 (1.75%, red), grange gas is Fig. 8

Integrating a radiative divertor with a high-performance core plasma leads to a complex interconnected phenomena in the SOL, pedestal that needs to be understood for reliable predictions. So that we can get a physics-based extrapolation of JET result to ITER and beyond, with whichever impurity necessary. An integrated team of specialists is working together to understand the complex picture of interconnected phenomena in the SOL, pedestal and core. The following three questions have been put forward to focus our current activities: Why is the density decreasing with neon seeding? How can we have density control with no ELM? What are the mechanisms reducing the ELM size?

**Pedestal MHD stability**: The reduction of the ELM size can only be addressed with a code such as JOREK. This is a longer-term project currently underway. However, the ELM trigger in these Ne-seeded plasmas is being addressed. The normalised pedestal pressure ( $\alpha$ ) and ideal MHD stability have been calculated with HELENA and ELITE and resistive MHD stability with CASTOR. From unseeded to higher neon-seeded pedestal,  $\alpha_{max}$  (max  $\alpha$ ) is reduced from 2.8 to 2; however, the decrease in the pedestal gradient is overcompensated by a widening of the pedestal width allowing higher pedestal pressure, see Fig. 10. Ideal MHD can explain the ELM trigger only in unseeded plasmas [24, 23], see Fig 15. Instead, with resistive MHD, both unseeded and Ne-seeded pedestals are near the stability within uncertainty [23], see Fig 15.

Edge modelling: One of the key questions to address is the drop of  $n_{e,ped}$  when neon is injected. This decrease of  $n_{e,ped}$  is the switch (in a successive set of events still to identify carefully) that allow recovery of a good confinement and high neutron rate starting from unseeded plasmas at high density. Although not shown in this paper, this drop of  $n_e$  in JET is more pronounced for neon than for other impurity such as Ar or N. For this reason, the reduction of  $n_{e,ped}$  is key to understand it, to know how to reproduce it in other devices with the appropriate impurity. Here, it is shown that it correlates with the improved confinement and neutron rates when operating close to the LH power threshold.

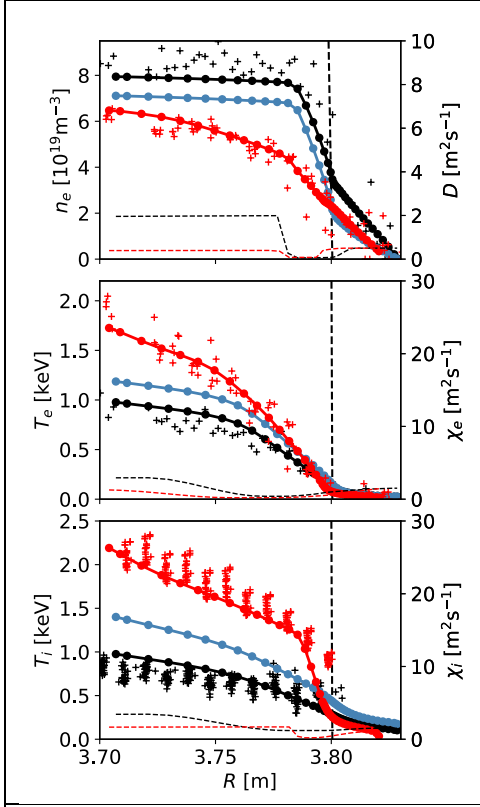


Fig 16: Upstream measured profiles (unseeded #103398 in black, seeded #103185 in red) are compared with SOLPS-ITER simulation (--o, with corresponding colours). The transport coefficients are shown in dashed lines. SOLPS code\_results with the same transport assumptions as #103398 and with neon-gas rate as in #103185 shown in blue.

Is the decrease of  $n_{e,ped}$  directly related to decrease in  $n_{e,sep}$ , or it there more than one process?  $n_{e,sep}$  is determined by the fuel recycling, i.e. strength of re-ionization in the divertor (and in parts at the main wall as well), in the case of JET, and transport in the near SOL. This decrease of  $n_{e,ped}$  is also an indication of a change of source within the pedestal which is determined by the flow of neutral crossing the separatrix and charge-exchange in the pedestal, and as some relation with  $n_{e,sep}$ . The balance of fuelling into and particle transport out of the pedestal is setting  $n_{e,ped}$ .

To assess the role played by the SOL and divertor/wall in the decrease of ne,sep in partially detached conditions, edge models are used such as SOLPS-ITER, SOLEDGE, EDGE2D-Eirene. Here we present results from SOLPS-ITER with ExB, grad-B and diamagnetic drift flows activated. It was possible to obtain a fair agreement between code and experiment for the unseeded discharge (#103398) and seeded discharge (#103185, same D-gas with  $\Gamma_{\text{Ne}}$ = 1.6x10<sup>22</sup> el.s<sup>-1</sup>) at the divertor target and the mid-plane profiles using the ion and electron input power at the inner boundary as calculated from TRANSP. The assumed levels of transport were quite low, i.e. close or below neoclassical limits. Without any change of transport assumption in the divertor, SOL or pedestal in the code from the unseeded case, neon is injected to level similar as in #103185 (1.6x10<sup>22</sup> el.s<sup>-1</sup>), and it is seen that a similar reduction of ne, sep is obtained experimentally (from 3.8x10<sup>19</sup> to 2.6x10<sup>19</sup> m<sup>-3</sup>), see Fig. 16. This corresponds to a drop of ionisation source within the simulation region from 1.1x10<sup>24</sup> to 6.3x10<sup>23</sup> s<sup>-1</sup>. n<sub>e,ped</sub> does drop but by only 10 % in comparison to 35% seen in the experiment. A change in pedestal transport is needed in addition to drop of n<sub>e,sep</sub> (Fig 16). A similar investigation was done SOLEDGE and EDGE2D-EIRENE and even though the

ionisation source within the pedestal and the pedestal transport differs for the unseeded pulse, the same observation can be made. In the end the drop of n<sub>eped</sub> is partly related to the change of conditions in the SOL/divertor and partly due to a change of transport in the pedestal from an unseeded plasma to the seeded plasma. At present, the edge models are being further refined against spectroscopic data to constrain the degree of freedom from the predicted recycling and neutral distribution to better quantify the ionisation source within the pedestal and the part played in the reduction of n<sub>e,sep</sub> by the divertor (i.e. power starvation due to the presence of radiation loss by seeding and thus leading too less available energy to ionise particles in the divertor) or by the wall.

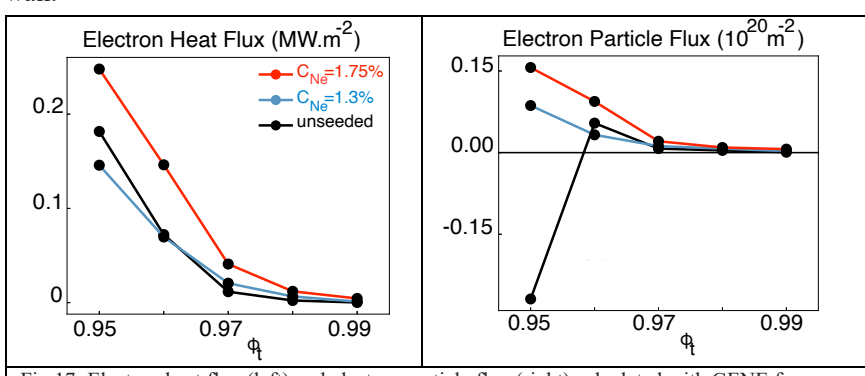
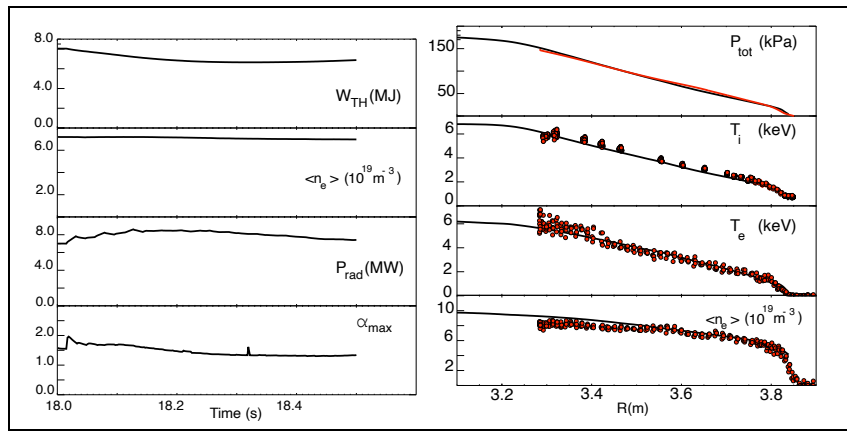


Fig 17: Electron heat flux (left) and electron particle flux (right) calculated with GENE from non-linear local simulation for #97481 (unseeded), #97482 (seeded,  $C_{Ne}$ =1.3%), #97490 (seeded,  $C_{Ne}$ =1.75%)

**Pedestal** Gyro-kinetic studies on the unseeded and neon-seeded JET-ITER baseline have been carried out with GENE [32, 33] to understand the key changes in the pedestal transport with the injection of neon, see Fig.17. Considering plasma composition as well as the profiles, the non-linear local GENE results show the change of transport from the unseeded plasma to the highest Ne-seeded plasmas

has two main components: the heat transport is increased at high  $C_{\text{Ne}}$ , due to an increased electron-scale (ETG) transport. The key reason is the increasing value of the ratio  $T_i/T_e$  as  $C_{\text{Ne}}$  is increased; The second key component is the change of particle transport from inward to outward from an unseeded plasma to Ne-seeded plasmas. The low value of the ratio  $T_i/T_e$  at low seeding generates an inward particle flux at the pedestal top due to low wavenumber ITG turbulence, possibly leading to a higher pedestal density. Local and global simulations (GENE) are in progress to quantify the latter point. In other words, in addition to the decrease in  $n_{e,sep}$  due to the injection of neon in the divertor, there is an additional decrease of the  $n_{e,ped}$  due to change of particle transport in the pedestal.



18: JINTRAC-Coconut-QuaLiKiZ results for #97490: (on the left) from top to bottom, thermal stored energy, average electron density, radiative power, and maximum normalised pedestal gradient; (on the right) experimental data in red and code result in black for total pressure, ion and electron temperature and electron density at 18.5s.

# Integrated modelling with Qualikiz-JINTRAC-

Coconut: Although features of the relevant physics are observed in unseeded and Neseeded plasmas, confirmation requires reproducing the key experimental results with a fully integrated model (coreedge-SOL/divertor).

As mentioned above, we are currently working on improving the edge description of the unseeded and Ne-seeded plasmas to integrate a more realistic EDGE2D-EIRENE solution to the core modelling with

JETTO with an anomalous transport calculated with TGLF. This work will be presented in future conferences. An intermediate step is to investigate whether it is possible to establish a stationary plasma with the standard EDGE2D-Eirene settings used in COCONUT, with a similar neon content, kinetic profiles, stored energy and normalised pedestal gradient as #97490. The pedestal width is imposed from the experiment, apart from the ETG related transport, the transport calculated by Qualikiz is reduced by a factor 3 in the ETB region as a proxy for the ExB stabilisation. It is found that a stationary simulation can be obtained with a Ne content, kinetic profiles, stored energy close to the experimental profiles, and normalised pedestal pressure gradient below the ideal PB stability limit, therefore compatible with small ELMs, with small extra transport imposed at the separatrix which may be also related to the use of QualiKiz. Future simulations with TGLF will clarify this point. The transport obtained in the ETB is within the same ballpark as calculated from the GENE for #97490. This indicates that ETG-related transport in the pedestal can enable stationary, high-performance operation with a reduced pedestal gradient—compatible with no or small ELMs (normalized pressure gradient below the ideal PB limit)—provided the pedestal width is sufficiently large.

### 5. CONCLUSION

A high-performance stationary Ne-seeded scenario with no ELM ( $\Delta T_{OuterTarget.max}$ <0°C) has been demonstrated in JET-ILW in D and D-T plasmas at 2.5MA and 3MA with high-recycling and partially detached divertor conditions and close to the power threshold. The operational space using a high-triangularity shape is accessible at  $P_{sep}/P_{LH}$ > 1.25 and at  $n_{e,sep}\sim2x10^{19}$  m<sup>-3</sup>, as seen at medium and high current, in D-D and D-T operation. Adding Neon suppresses the ELMs ( $\Delta T_{OuterTarget.max}$ <20°C) and reduced the electron separatrix density (via a reduction of the ionization source) and the pedestal density. In terms of understanding, the latter would require in addition a modified level of pedestal transport, possibly linked to a particle flux reversal. Given the importance of a scenario that meets key requirements for ITER and for future power plants, these effects are required to be disentangled for robust predictions. An integrated team of specialists is currently advancing this topic.

This work has been carried out within the framework of the EUROfusion Consortium, partially funded by the European Union via the Euratom Research and Training Programme (Grant Agreement No 101052200 — EUROfusion). The Swiss contribution to this work has been funded by the Swiss State Secretariat for Education, Research and Innovation (SERI). Views and opinions expressed are however those of the author(s) only and do not necessarily reflect those of the European Union or the European Commission or ITER. Neither the European Union nor the European Commission nor ITER can be held responsible for them.

References: [1] R.A. Pitts et al, Nuclear Materials and Energy 20 (2019) 100696 [2] C. Giroud et al 2024 26th Int. Conf. on Plasma Surface Interaction (Marseille, France) [3] Carvalho I S et al 2024 50th EPS Conf. on Plasma Physics (Salamanca, Spain) [4] C. Giroud et al., Plasma Phys. Control. Fusion 57 (2015) 035004 [5] Giroud C et al 2021 28th IAEA Fusion Energy Conf. (Virtual Event, 10 May-15 May 2021) [EX/3-9] [6] Martin Y.R. and Takizuka T. (ITPA CDBM H-mode Threshold Data Group) 2008 J.Phys.:Conf.Ser.123 012033 [7] Giroud C. Nucl. Fusion 64 (2024) 106062 [8] Fajardo D, IAEA FEC 2025 TH-C [9] Vartanian S. et al 2021 Fusion Eng. Des. 170 112511 [10] Klepper C. et al 2020 Nucl. Fusion 60 016021 [11] Neverov V., Kukushkin A.B., Kruezi U., Stamp M.F. and Weisen H. 2019 Nucl. Fusion 59 046011 [12] Lombardo J. Nucl. Fusion 65 (2025) 096009 [13] Zotta V. et al 51st EPS Conf. on Plasma Physics (Vilnius, Lituania) [14] Andersson Sunden E. Nucl. Instrum. Methods Phys. Res. A 610 (2009) [15] Linus Hagg et al 2025 Plasma Phys. Control. Fusion 67 035024 [16] Garzotti L et al et al 51st EPS Conf. on Plasma Physics (Vilnius, Lituania) [17] C. Bourdelle et al 2018 Nucl. Fusion 58 076028 [18] Huber A. private communication [19] Fajardo D. private communication [20] Fajardo D., Plasma Phys. Control. Fusion 67 (2025) 01502 [21] Kumpulainen H. IAEA FEC 2025 TH-C [22] Alessi E. et al. 2024 50th EPS Conf. on Plasma Physics (Salamanca, Spain)[23] Nystrom H. submitted to Nucl. Fusion [24] Sos M. submitted to PPCF [25] M. Marin et al 2023 Nucl. Fusion 63 016019 [26] Leoni C. et al 51st EPS Conf. on Plasma Physics (Vilnius, Lituania) [27] Hu Q et al, Nuc. Fusion in preparation [28] Ryan P. paper in preparation [29] Silvagni D Nuclear Materials and Energy 42 (2025) 101867 [31] Solano E. Nucl. Fusion 63 (2023) 112011 [32] Jenko F., Dorland W., Kotschenreuther M. and Rogers B. 2000, Phys. Plasmas 7 1904-10 [33] Görler T., Lapillonne X., Brunner S., Dannert T., Jenko F., Merz F. and Told D. 2011 J. Comput. Phys. 230 7053-71 [34] Litaudon X. IAEA FEC 2025, fig. 5 [35] Rigamonti D. et al 2024 Nucl. Fusion 64 016016 [35] Nocente M. et al Rev. Sci. Instrum. 93, 093520 (2022) [36] Eich T., Nucl. Fusion 61 (2021) 086017 [37] Svoboda J. et al 2021 JINST 16 C12015